10. Secondary Cratering

It is commonly accepted that impact crater populations on solid–surface planetary bodies predominantly reflect the impacts of a generally known impacting population. As outlined in the previous chapters, this fact is used to estimate relative and absolute surface ages. In the 1960's (e.g. Fielder, 1962; Shoemaker, 1965), the existence of rayed craters and secondary crater clusters in the near–field of craters on the Moon was observed. The shape of the crater size–frequency distribution and therefore the distribution of the projectile population has been topic of discussions. It has been suggested that the observed lunar cratering recored is "contaminated" by an indeterminable number of secondary craters. The discussion to what extent the crater frequencies in the smaller–size range ($D \leq 1$ km) is caused by primary or secondary cratering, includes a discussion of what is the "true" shape of the primary crater or projectile distribution. This also implies whether or not a surface age determination based on crater counts is possible. In the following it will be discussed what secondary–crater contribution is generated by a primary crater population. The shape of the assumed crater production function is given by a power–law description of $N \sim D^{-2}$, N is the cumulative number and D the diameter.

Secondary cratering is observed especially in the closer vicinity of the primary impact crater. These secondary craters are part of the ejecta pattern and characteristically form clusters or chains. The chains are known as herringbone (ejecta) patterns (Wilhelms, 1976; Wilhelms *et al.*, 1978) or, over larger distances, are associated with crater rays which are related to albedo features spanning large amounts of the lunar globe. For age determination based on crater counts, craters belonging to these secondary cratering phenomena, are recognized and eliminated from the counts. For ambiguous situations, where it is not possible to clearly distinguish primaries and secondaries, crater counts naturally are impracticable.

The fact that secondaries can travel far distances and produce craters without any characteristic spatial distribution (clusters or chains), or typical ejecta patterns, challenged age dating technique based on crater count. The unknown contribution unrecognized global secondaries (termed "background secondaries" by Shoemaker (1965)), craters outside identifiable crater clusters and chains, has been discussed to violate the method of surface age determination based on crater counts in the smaller–size range.

Advocators against a steep primary crater size–frequency distribution believe that the observed crater size–frequency distributions is the result of a primary crater distribution reflected by a cumulative -2–sloped power–law (assuming a cumulative distribution of $N \sim D^{-2}$) and a superimposed secondary distribution reflected by a power–law in a slope–index range higher than the primary. For such a piecewise power–law description is argued on observations of the projectile distribution (asteroid belt and near–Earth asteroids), although detailed observations at the smaller size range of the asteroid population are still lacking, and allows speculations about the numbers of smaller bodies (below 1 kilometer in diameter), capable of producing craters below about 10 kilometers in diameter.

The arguments in favour of a steep primary crater size–frequency distribution are summarized in Section 10.1.2.

Nevertheless, due to the newly available image data of the THEMIS instrument, the old debate concerning the influence of secondary cratering (craters produced by the ejecta of a primary impact event) has been raised once again. McEwen *et al.* (2003) and McEwen

(2003) describe a fresh–appearing 10–km diameter crater at 7.7° N and 166° W that should have produced a huge number of very small craters, possibly covering its distant surroundings. The authors conclude that the steep branch of the crater–production function would be highly influenced by secondary cratering for craters smaller than 1 km.

10.1. Remote Secondary Cratering: The Zunil Case

The effect of secondary cratering on age determination is discussed with respect to the discovery of the 10–km Zunil crater, which is located in the Cerberus plains (Cerberus Planitia/Athabasca Valles region) of Mars and surrounded by a large field of secondary impact pit clusters that can be seen up to radial distance of 1000 km from the main impact crater (McEwen, 2003; McEwen *et al.*, 2003, Fig. 10.1). McEwen *et al.* (2005a) conclude that crater retention ages based on the small–crater range (below about 300 m for young surfaces) could be under– or overestimations of surface ages, thereby making age determinations of this size range unreliable. Especially, if only high–resolution images are available, age determination would be close to impossible, since the issue of distinguishing primaries and secondaries is not fully resolved.

This conclusion ignores the fact that the assumed primary distribution has been measured independently on the Moon, in the asteroid belt (e.g. on Gaspra), which is the source region of the inner solar system projectile (impactor) population, and as here discussed has been measured on Mars.

An argument in favor of a primary small–crater distribution stems from the source region itself, the asteroid belt. Two asteroids, Gaspra and Ida, have been observed during the Galileo flyby. Particularly, Gaspra data fit the lunar standard crater production function and show the steep size–frequency distribution (Neukum and Ivanov, 1994; Chapman *et al.*, 1996; Ivanov *et al.*, 2001). This is direct confirmation that the steepness at small crater sizes ($D \leq 1$ km) is an effect of the primary impactor size–frequency distribution and not an effect of secondary crater admixture at small sizes.

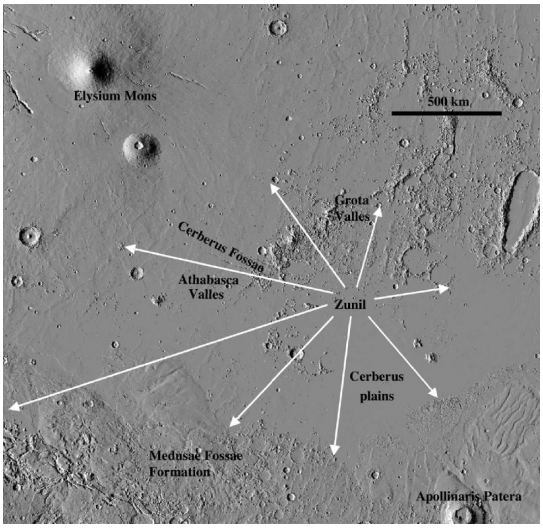

Figure 10.1.: The extent of Zunil's secondary strewn field in the Cerberus plains as described by McEwen *et al.* (2005a).

Additionally, bolide frequencieshitting the Earth atmosphere (fire balls) have been transferred to lunar impact conditions and plotted on the measured lunar crater size–frequency distribution. They fit within a factor of two (Ivanov, 2005). More controversial, but supporting the idea of a "steep" distribution, are predictions of the number of near–Earth asteroids, that is the impactor population for the Earth and the Moon. It fits the measured lunar crater size–frequency distribution. Werner *et al.* (2002) show that the size–frequency distribution of a time–averaged projectile population derived from the lunar crater size–frequency distribution (Neukum and Ivanov, 1994) provides a convincing fit to the size–frequency distribution of the current near-Earth asteroid (NEA) population, as deduced from the results of asteroid search programs. These results suggest that the shape of the size–frequency distribution of the impactor flux has

remained in a steady state since the late heavy bombardment and that the steep distribution is primary.

All these measurements are in good agreement. Therefore, the suggestion by McEwen *et al.* (2005a) of an underestimation of surface ages using crater frequencies is untenable. The relevant projectile groups support the steep branch as observed in the crater record.

Bierhaus *et al.* (2005b) and Bierhaus (2004) report their findings of secondaries in a sizable fraction on the jovian moon Europa. Nevertheless, they observe crater size–frequency distributions which show a great variety of slopes, and indices are ranging between -2.5 and -5 for cumulative distributions. These slope ranges are common for crater production function and also secondary crater distributions. It appears that they ignored any geologic unit boundaries, therefore, they were not able to define any reliable production function, but could show that these units are "contaminated" by different amounts of secondaries. Remarkably, the small–crater record show strong clustering, which is their only reasoning to claim that they are dominantly secondaries.

Their observation is made in a dynamically different Solar System regime with respect to the projectile source (possibly dominated by comets) compared to the inner Solar System regime (dominated by asteroids). They agree that in the inner Solar System small craters are also formed by small impact projectiles that are not observed in the Europa case. Nevertheless, they claim that the ratio of primaries to secondaries is unknown.

Hartmann (2005) presented a detailed discussion on whether these findings imply that the steep branch of the small–crater distribution is dominated by primaries (impacts from interplanetary bodies) or by secondaries (impacts of fall-back debris from larger primaries). He concluded that clustered secondaries are generally not included in crater counts and that crater counts made in geological context have more constraints than just the crater frequencies. The steep branch at small crater sizes was

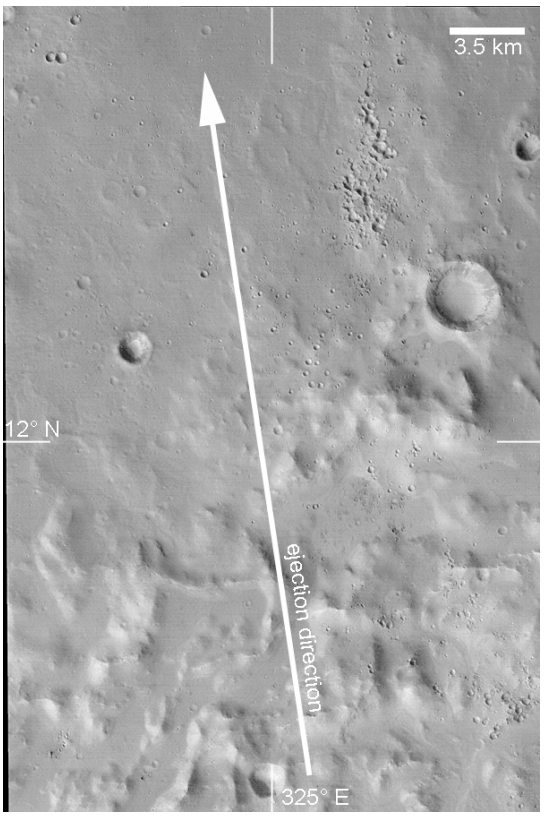

Figure 10.2.: Example of clustered secondary craters around 13° N and 325° E, observed in orbit 2024 by the HRSC experiment. These clusters were produced by crater Mojave which has a diameter of about 57 km and is located in a distance of roughly 500 km south at 7.5° N and 327° E.

recognized on asteroids by Neukum and Ivanov (1994) and Chapman *et al.* (1996) and confirms that small lunar and Martian craters originate from an interplanetary asteroidal primary projectile source, and already having a steep distribution.

The steep small–crater branch on Mars and the Moon might have an admixture of unrecognized secondaries. Hartmann also argues that determining ages, those secondaries are part of the signal. Using the crater counts over the widest possible diameter range, ages can be determined by the fit of the entire distribution and not only at one point or a small range. Ages are reflected in the distribution isochrons and can

also be reliably determined from small–crater distributions, even if secondaries are admixed.

10.1.1. Characteristics of the Zunil secondary strewn field

We do not deny the existence of unrecognized global secondaries. There are cases where a separation of primary impact craters and endogenic or secondary craters is impossible and an age determination based on crater frequencies can be carried out. Fig. 10.2 show a prominent example of secondary crater clusters stemming from the 57–km–diameter crater Mojave roughly 500 km south of it. Nonetheless, stratigraphic relations yield insights into the general regional geologic evolution. Exluding the clustered units, studying the geologic evolution not only based on stratigraphic relation, but also on crater counts, is possible. From our experience, admixture is low in most cases, probably on the order of less than 10%. The validity of this statement is examined in detail in Chap. 10.3 (below).

In order to shed further light on this subject, we have performed a detailed examination of the crater populations in the Cerberus plains area, and which has been discussed by McEwen *et al.* (2005a). They used the fact that the secondary population of the Zunil secondary strewn field exhibits a prominent black halo, and the discovery could occur as a result of distinction from the primary population and secondary population. The HRSC experiment has covered the part of this plain (HRSC orbit 1152) where most of the clearly identifiable secondary craters of Zunil have impacted (Fig. 10.3a). In a radial distance of about 300 km from crater Zunil, we have measured on a uniform geologic unit the crater size–frequency distributions for (mostly) primaries and for the proposed secondary craters. Fig. 10.3 shows the resulting crater size-frequency distributions of the primary (Fig. 10.3b) and the secondary (Fig. 10.3c) population. Further contamination by secondary cratering can almost be excluded because of the young age of the unit. The secondary population has a much steeper distribution (red curve) than the Martian crater production function (black curve). This was already observed for near– and far–field secondary crater populations on the Earth's Moon, (e.g. König, 1977; Vickery, 1986) and is in agreement with the observations by Bierhaus *et al.* (2005a,b) for the jovian moon Europa.

If an inexperienced observer measures craters in areas of the Cerberus plains, unwittingly including secondary craters in his measurements, he would achieve the distribution shown in Fig. 10.3d. Investigating the separated primary and secondary crater size–frequency distributions in detail (based on the frequency tables) one observes a crossing diameter at which the number of secondaries exeeds the number of primaries (for detailed discussion see Sec. 10.2.1). At diameters less than 150 m the number of proposed secondaries exceeds the number of primaries by a factor of up to five, while below the number of primaries is double. This observation is in agreement with observations made by König (1977), see below. Based on this observation and utilizing the theoretical approach outlined in Chap. 10.2, one could derive the size of the generating primary crater, which would be around 5 km, smaller than Zunil. If an experienced observer investigates the crater size–frequency distribution of summed secondaries and primaries (Fig. 10.3d), at small sizes (below 150 m), the distribution still appears slightly steeper than the Martian production function. Nevertheless, an experienced observer would recognize the slightly higher steepness and in all likelihood, judge the distribution contaminated by secondaries, thereby carefully inspecting the measurement area for possible further elimination of the secondary craters from the measurement.

This example also illustrates that the proposed factor of at least 20 (McEwen, 2003) is not reached at all, but at most yields a factor of two in age. This is an acceptable error in crater counts for young ages, as pointed out by Hartmann (2005).

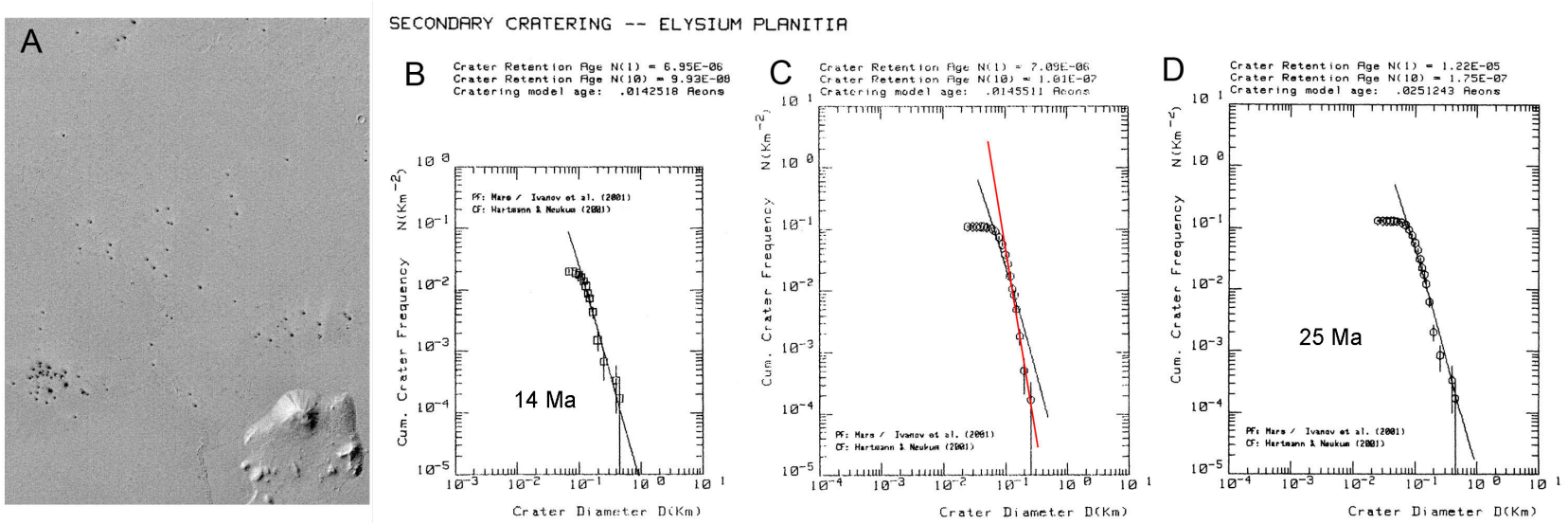

Figure 10.3.: During the MarsExpress orbit 1152 the HRSC experiment has covered part of the Cerberus plains where most of the well identifiable secondary craters of Zunil impacted (A), the image shows a region of 30 km x 35 km. It is easy to separate the primary and secondary population due to the prominent black aureole of the secondaries. (B) shows the resulting crater size-frequency distributions of the primary and (C) the secondary population. The secondary population has a much steeper distribution (red curve; for comparison the Martian crater-production function, black curve) as has been observed already for the Earth's Moon. The crater size–frequency distribution in Fig. (D) demonstrates a situation if both populations (primary and secondary) were measured together. Still the distribution appears slightly steeper at very small sizes than the Martian production function. Fitting the crater production function for Mars it is possible to determine the age of the primary and the mixed population measurement (B and D). The resulting ages differ by a factor of less than two, which shows that crater counts yield absolute ages of tolerable error (of the same order of magnitude) even if secondary craters were included unwittingly.

In our test case areas (Athabasca Valles, Chap. 12), we could rule out the influence of secondary crater admixture. Measured crater size–frequency distribution in areas of different ages show the same the steepness of the size–frequency distribution in the small diameter range (less than 100 m). If secondary crater contamination would influence the distributions, a change in the steepness of the distribution would be observed at differently aged surfaces depending on the relative amount of contributing secondary and primary craters, which depends on age. This has not been observed.

10.1.2. Reasoning for a steep primary crater size distribution branch

The arguments for the steep–slope branch produced by dominantly a primary projectile distribution at the small size range (below about 1 km) can be summarized as follows:

- a steep crater size–frequency distribution is observed on bodies (e.g. Gaspra) in the asteroid belt, the projectile source region
- clusters, chains and even distant secondaries (such as in the Zunil case, which appear clustered too !) can be excluded in measurements
- steep distributions according to the crater production function are observed on Mars and the moon for differntly aged surfaces
- fireball observations (small projectiles hitting the Earth's atmosphere) scaled to cratering the moon show the expected slope steepness (of the crater production function)
- near–Earth asteroids size–frequency distributions (deduced from detection statistics) show the same steep slope. They are the projectile population of the moon and Earth.
- measurements on the moon and Mars in different geologic but homogeneous units always fit the crater production function
- erroneously included secondary craters could lead to an overestimation of surface ages by less than a factor of 2

To finally understand the possible contribution of globally unrecognized background secondaries to the crater production function, here, a crater distribution is constructed based on commonly raised arguments. The resulting distribution is compared with observations.

10.2. Gedankenexperiment: Secondary Cratering

Shoemaker (1965) stated that the primary cumulative distribution follows a power–law of $N \sim D^{-2}$, and this is used as the basic distribution of this experiment. We assume that a global population of unrecognized secondary craters exists, which is responsible for the change in slope towards smaller crater diameters. They are randomly distributed and not distinguishable from primary craters, and produce the slope of the observed crater size–frequency distribution at crater diameters below about 1 kilometer (with slope indices between -3.5 and -3.0). We ignore how much ejected material volume is deposited near the primary crater. We use measurements of near–field secondaries to characterize the unknown far–field distribution: The largest secondary crater around a primary has a crater diameter of about 5 % of the primary one. Observed near–field secondaries show well–documented distributions (clusters and chains) at the larger size range, given by power–law descriptions with cumulative slopes of –4± 1, (e.g. König, 1977; Vickery, 1986). Nevertheless, measurements by Vickery (1986) give an erroneous impression, since they do not cover the smaller–size range of the secondary crater distribution, where a bending to a flatter distribution is firmly observed (König, 1977).

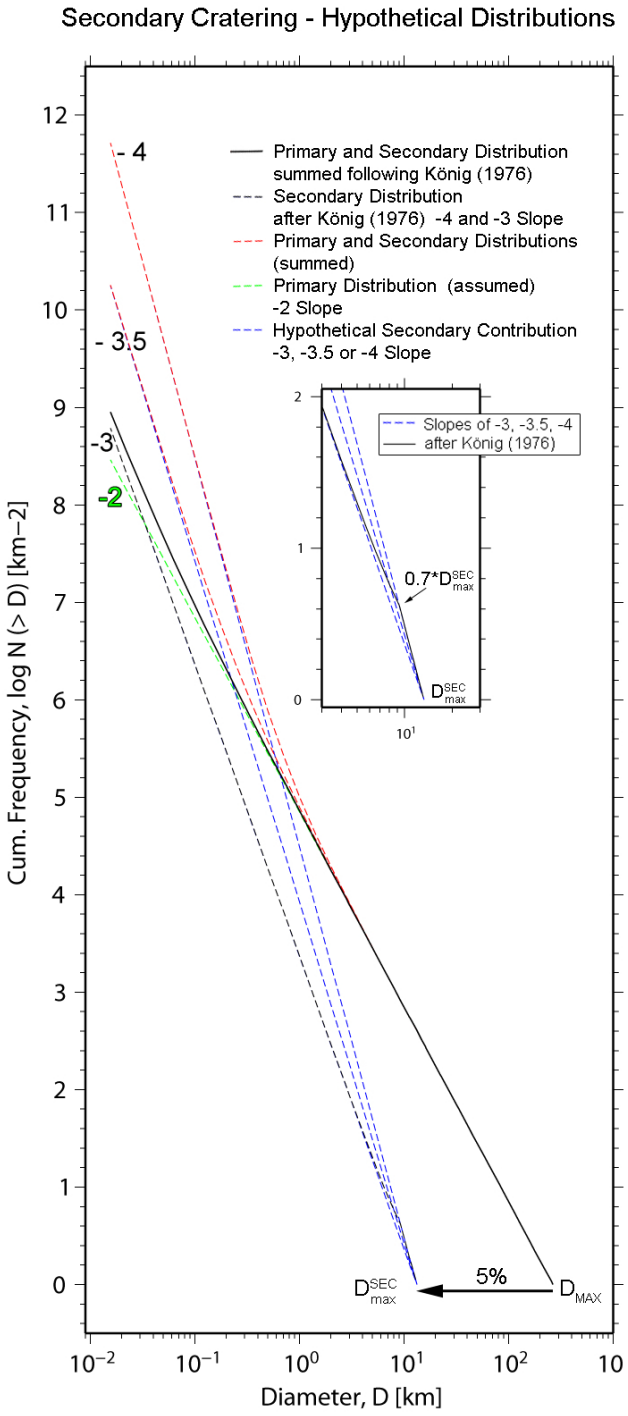

Figure 10.4.: The construction of a hypothetical crater size frequency distribution for Mars, where the global surface is assumed to be 1 Ga old. Different crater distributions are shown: an assumed primary distribution with a slope index of -2 (dashed green), three hypothetical secondary distributions with slope indices of -3, -3.5, and -4 (blue dashed), a secondary crater curve following observations by König (1977) (black dashed). The inset enlarges the important region to display the difference between the latter approach and a pure -3 sloped distribution, for details see text. The summed assumed –2–sloped primary and the individual (slope indices of -3, -3.5, and -4) secondary distributions are given as dashed red and solid black curve, respectively.

The slope steepness with an index around –4 is in contradiction to the observed crater size–frequency distributions, which show cumulative slopes of between -3.5 and -3.0 at crater diameter ranges below 1 kilometer. Such a discrepancy has to be resolved.

The physics of processes such as impact cratering (crushing or grinding) are described by simple conservation constraints for mass, momentum, surface energy and kinetic energy. Naturally, the fragmentation occurring during a single impact event limits the production of secondary projectiles by its available volume and impact energy. It is clear that a very steep power–law distribution cannot continue to arbitrarily small fragments, but there is a cut off at which the number of fragments decrease rapidly. This effect has been observed in grinding or crushing experiments and is known as Rosin–Rammler or Weibull–distributions describing a processes at any scale (see for example Brown and Wohletz, 1995). Weibull–based Grady–Kipp models have been commonly used as models in fracturing–related processes (e.g. cratering (Melosh *et al.*, 1992), volcanic ash production (Wohletz *et al.*, 1989) or asteroidal collisions (Michel *et al.*, 2001)). Generally, a lack of smaller particles has been observed. König (1977) investigated near–field secondaries around lunar rayed craters Aristarchus, Kepler and Copernicus in detail. Measuring crater densities and size–frequency distributions in chains and clusters at different distances from the primary crater, she found distance–independent crater size–frequency distribution curves, which can be described by two straight lines in a double-logarithmic scheme. They are represented by a power law given by $N \sim D^{\alpha}$ ($\alpha = -2.5 \pm 0.3$) in the smaller diameter range and for larger craters a power law given by $N \sim D^{\beta}$ ($\beta = -4 \pm 1$). The transition diameter D_A at which the steep and flat branch of the distributions merge is related to the largest observed secondary crater D^{sec}_{max}. Summarizing her findings, we can characterize secondary crater distributions having a general form of:

$$N^{sec}_{cum} \sim D^{\alpha}$$

The largest secondary crater controls the transition diameter:

$$0.7 \cdot D^{sec}_{max} \sim D_A$$

The power–law segments are given by
$D^{sec}_{max} > D > D_A$ where $\alpha = -4 \pm 1$
and
$D < D_A$ with $\alpha = -2.5 \pm 0.3$.
Based on the observations and this knowledge, the slope steepness contradiction mentioned above, is solved.

Using the observations of König (1977), the secondary crater distribution characteristics are used to prepare a single master curve.

10.2.1. Construction of a hypothetical total crater distribution

For this exercise, the Martian surface is assumed to be globally 1 Ga old. Applying a cratering chronology model (Hartmann and Neukum, 2001) the largest primary crater derived through a distribution given by $N \sim D^{-2}$ is calculated. The largest crater is found to have a diameter of about 265 kilometer. In Fig. 10.4 all distributions which will be discussed here are given in a double–logarithmic scheme, the primary crater distribution is shown as a green dashed line. As a rough estimate the largest secondary crater which can be produced globally has a diameter twenty times smaller than the largest primary. This relation is shown in Fig. 10.4 for a globally 1–Ga-old surface. A largest secondary crater with a crater diameter of 13.25 km following $D^{sec}_{max} = 0.05 \cdot D_{max}$ is produced. At this point three possible secondary crater distributions are shown with slope indices –3.0, –3.5 and –4.0, (blue dashed lines). As discussed above, the –4–slope occurs for secondary craters only over a smaller size range between D^{sec}_{max} and $0.7 \cdot D^{sec}_{max} \sim D_A$ and continues as a cumulative curve with a slope index of at least –3.0, (black dashed line). This approach following König (1977) is shown in

greater detail by the inset. While a single impact generates a secondary distribution as observed by König (1977), the global cumulative distribution appears as enveloping curve of secondaries produced by the primary distribution. They must mimic the observed distribution (slope indices range between –3 and -3.5 at the smaller–size range), if the globally produced steep branch is only due to secondary craters. Generally, the frequencies between D_{max}^{sec} and the inflection point D_A are low. Therfore, such a distribution can be considered having a –3–slope in the smaller crater size range, shown in Fig. 10.4, where -3–slope distribution and the two segmented distribution are aligned. For comparison with an observed crater size–frequency distribution, the potential primary (assumed to have a –2–slope over the entire crater size range) and hypothetical secondary distributions are summed. The summed distributions are shown as red dashed curves, having secondary crater contributions given by -4– and -3.5– slope distributions. The sum of primary and secondary craters given through the König approach is depicted as solid black line. This approach is nearly identical with a -3–slope secondary contribution.

It has been discussed that the lunar size–frequency distribution of craters smaller than 3 km is consistent with secondary impact populations predicted for larger craters by Shoemaker (1965) and Brinkman (1966). Craters for which no specific primary craters can be identified were termed "background secondaries" by Shoemaker (1965). This idea was adapted by Soderblom *et al.* (1974) and later resumed by Neukum (1983). Soderblom *et al.* (1974) have shown that the slope for the entire secondary crater population is given by the same slope of the distribution of secondaries generated by a single primary. Furthermore, the secondary population naturally dominates the total crater population at the smaller size ranges (Fig. 10.4) given by the diameter at which the number of secondaries exceeds the number of primaries. This crossing diameter D_c is given by the relation:

$$D_c = D_{max} \left[\frac{\alpha}{(\beta-\alpha)k^{\beta}} \right]^{1/(\alpha-\beta)}$$

where D_{max} is the largest contributing primary crater, α is assumed to be –2 and β is discussed to range between –3 and –4 (see above). Soderblom *et al.* (1974) concluded that this crossing point between primary and secondary crater population curve for a given β = –3.5 is theoretically near 1 km crater diameter (and the largest primaries observed ranged around 50 km in diameters). Their comparison with the most pristine observed Martian crater distribution appeared to be approximated well by such a distribution. It shows that under fixed conditions (a specific time) one could derive such a relation. As will be discussed below, this relation is unstable for differently aged surfaces.

It has already been demonstrated by Neukum (1983) that if the steep branch were due to secondary craters superimposed on a flatter distribution (e.g. $N \sim D^{-2}$), then the steep branch of the distribution in total abundance of craters per size interval would be dependent on the amount of cratering of the surface by the flatter distribution and the occurrences of primary craters. This would lead to a dependence on exposure time, hence surface age, and would affect the distributions in such a way that the crossover diameter point (i. e. the diameter at which the steep and the flat part of the composed distribution on a log–log diagram cross each other) would move to larger diameters in the distributions measured on older surfaces.

Considering a primary production function given by $N \sim D^{-2}$, Fig. 10.5, top, show this dependence for the largest primary, and accordingly the largest secondary which would be generated assuming a primary production function with a –2–slope and a projectile flux following Hartmann and Neukum (2001). Naturally, the maximum diameter relation propagates in the crossover diameters given for three discussed slope parameters of possible secondary crater distributions, -3, -3.5 and -4, respectively (Fig. 10.5, bottom). The effect due to different surface ages on the resulting hypothetical total crater distributions are shown in Fig. 10.6 for

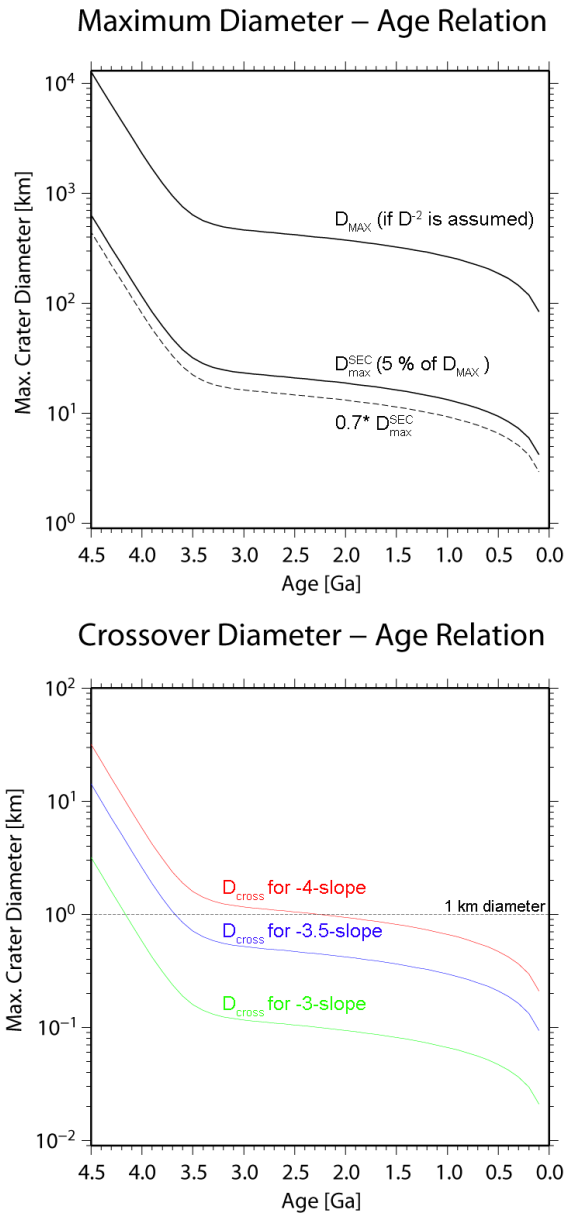

Figure 10.5.: Dependence of surface age and hypothetical maximum diameter, which would be observed on Mars having globally a single surface age (top). This age–dependence is reflected in the largest generated secondary and propagates in the cross–over diameter given (bottom) for three secondary crater distributions considered with slope indices of -3, -3.5, and -4, respectively. For details see text.

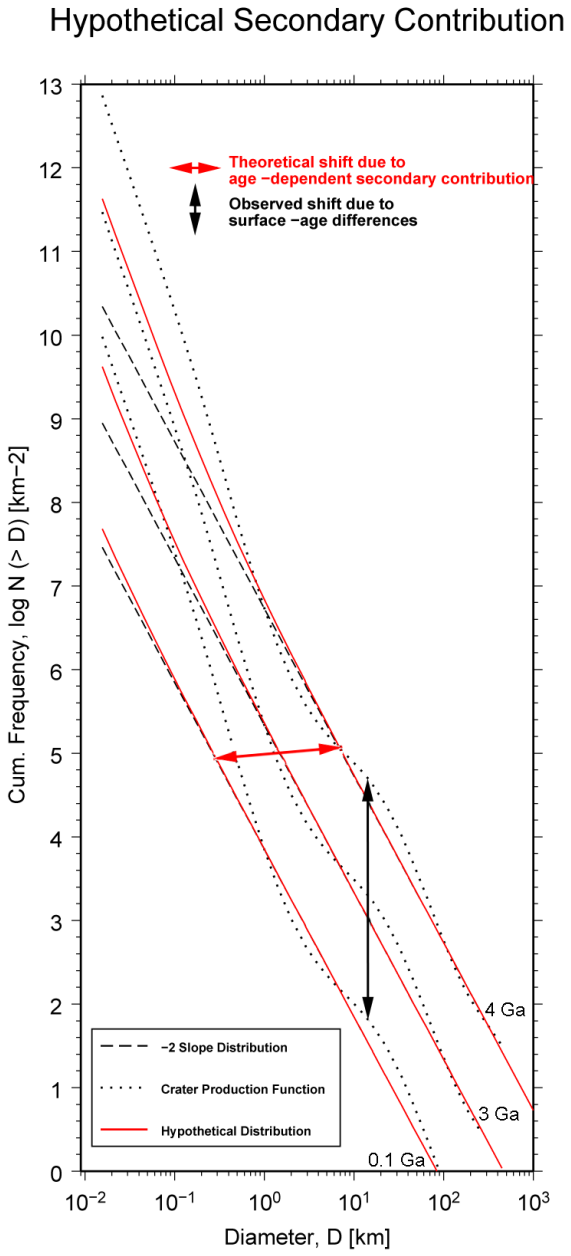

Figure 10.6.: Demonstration of the age–dependence on the hypothetical total crater size–frequency distribution for three different surface ages at global scale (red curves at ages of 4 Ga, 3Ga, 0.1 Ga) in comparison with the Martian standard crater production function for analogous ages. While in reality only a frequency shift is observed, the hypothetical distribution mainly varies in diameter direction.

surfaces of an age of 4 Ga, 3 Ga and 0.1 Ga (red curves).

Obviously, the effective onset of the secondary crater branch is propagating towards larger diameters with growing surface age. What we find in all measurements on the moon or Mars, instead, this point (in observed crater size–frequency distributions) appears at a single diameter value irrespective of the counting area, age and number of large craters. This is a very powerful argument for a primary source for both the flat and steep part of the size–frequency distribution. For comparison, the crater production function for Mars as discussed in Chap. 5 is plotted for analogous ages.

The slope change between a flatter branch (considered as primary) and the steeper branch (considered as secondary–dominated) is the key to the judge, which interpretion reflects reality: Neither on the moon nor on Mars a shift towards larger crater diameters is observed. Numerous measurements gathered and described in the following chapters confirm this for the Martian case, for examples see Chap. 11.

10.3. Hypothetical Secondary–Crater Contribution

The most recent dataset obtained by the HRSC, complemented by Viking, THEMIS and MOC in which crater frequencies over the full crater–size range can be determined, the steep distribution branch is visible and fits the Martian crater production function (and agrees with the lunar one, see Chap.5) over the full size range and for differing surface ages (for further discussion see Chap. 11). Therefore, it is likely that the contribution of theoretically possible background secondaries is minor. To better judge the real amount, predicted secondary crater distributions are compared with the Martian standard distribution. Based on the arguments outlined above the contribution of secondary craters to the total crater number observed and represented by the Martian standard crater production function cannot be the majority at the small size range crater numbers.

Following the theoretical consideration to describe possible secondary crater distributions (after König (1977)), their numbers as a function of surface age are estimated and compared to the observed crater production function. Therefore, the secondary crater curves and Martian crater production functions are calculated in age steps of 0.1 Ga. The secondary crater curves are prepared assuming a –3.0– and a –3.5–slope for the continuation after the inflection point defined by $0.7 \cdot D_{max}^{sec} \sim D_A$. For both distributions, analytical expressions are used. The portion of secondary craters is given through the ratio between the cumulative total crater number determined through the Martian crater production function and the estimated total number of secondaries, respectively. Fig. 10.7 shows the colour-coded ratio for an assumed –3.0–slope index (top) and a –3.5–slope index (bottom). Secondary crater percentages which exceed the number of primaries by 160 % are plotted in dark red and for detailed understanding 1 % to 5 % isolines are plotted in the dark blue areas.

As already discussed in the earlier chapters, the hypothetical contribution of secondaries, assuming a –3.5 slope index, outnumbers the observed Martian crater frequencies for old surfaces (older than 3.6 Ga) which is not observed. Therefore, the probability that this assumption is correct is very low and would contradict detailed investigations made in secondary crater clusters and chains (see e.g. König (1977) or Vickery (1986). Nevertheless, if one want to be cautious: Crater frequencies determined in a diameter range larger than 5 km at any age, almost no secondary contamination are observed. For both slope indices crater counting operates well above the cross–over diameter at which the number of secondaries equals the number of a hypothetical flat primary distribution (given by $N \sim D^{-2}$). Also at young surfaces (less than 2 Ga) saturation is reached before the portion of secondaries would be dangerous (for the –3.5–slope case).

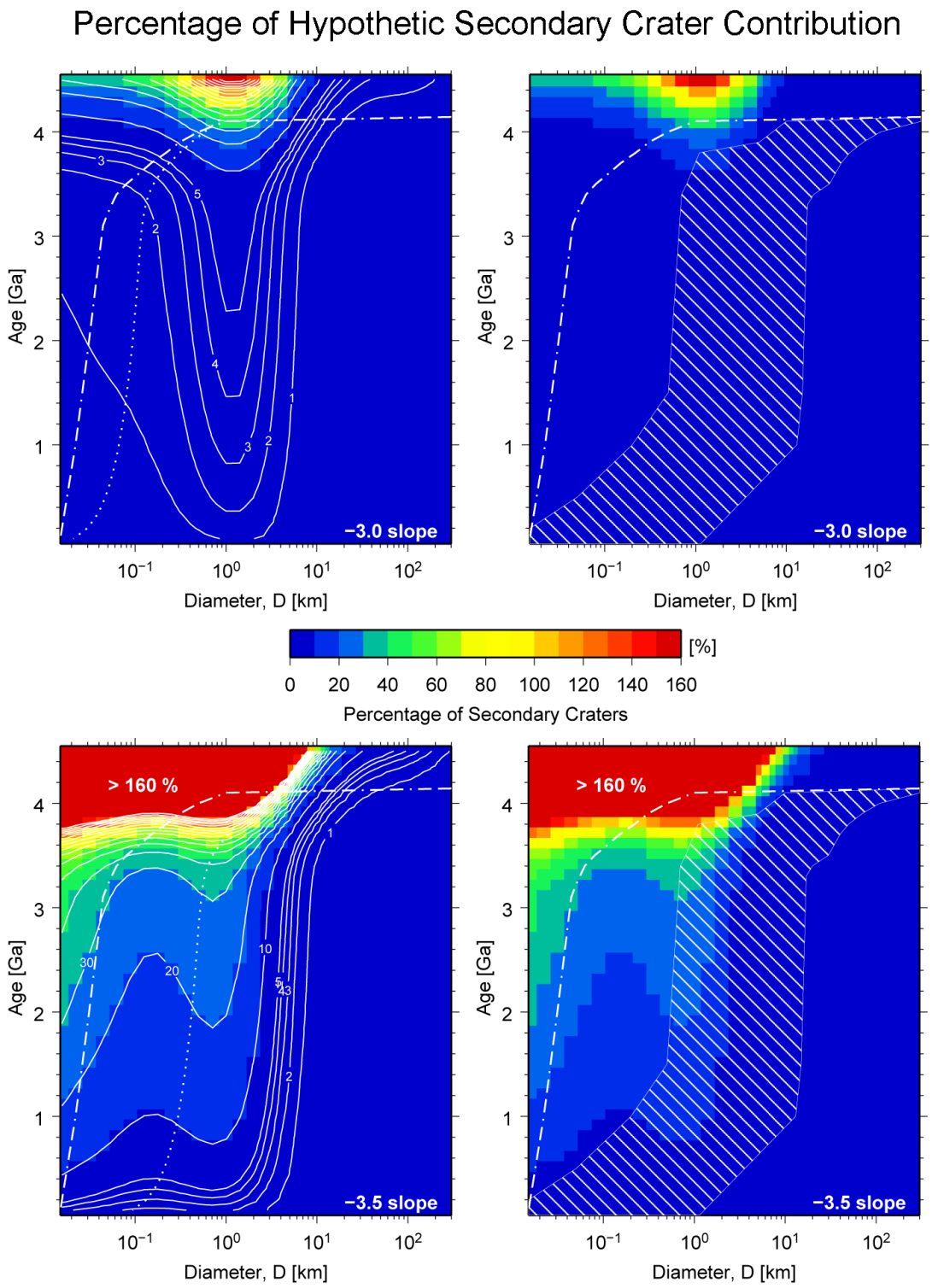

Figure 10.7.: The hypothetical contribution of secondaries assuming a -3–slope (top) and a -3.5–slope (bottom) compared with the Martian standard crater production function for varying surface ages, given as percentage of the primary function (left and right). The dashed curves indicate the saturation limit (left and right), the dotted curve indicates the crossing diameter (left) as shown in Fig. 10.5. The hatched unit (right) indicates the crater diameter range in which all measurements presented in this thesis were performed.

In the –3.0–slope case a "dangerous" region of contamination is never reached. An exception needs to be made for very old surfaces (above 4.0 Ga) if one attempts to determine ages through crater frequencies measured around 1 km. On Mars this is usually impossible, because erosion processes have acted on eliminating the cratering record at this diameter range. It is more likely that one would measure erosional surface ages than any secondary contamination produced by an ancient (older than 4.1 Ga) primary population. For the smaller size range the saturation limit is reached before the contamination exceeds 30 % . Even in these cases measurements at a broad diameter range allows for a reliable age determination.

It is interesting to note, that even in regions of low secondary contribution the diameter range around 1 km is "most" affected. Around 1 km diamter, in the Martian crater production function slope changes occur and the steep "secondary" contribution distribution and the steep primary branch run sub–parallel for a while. Therefore, especially for old surfaces, the "contamination" there is highest.

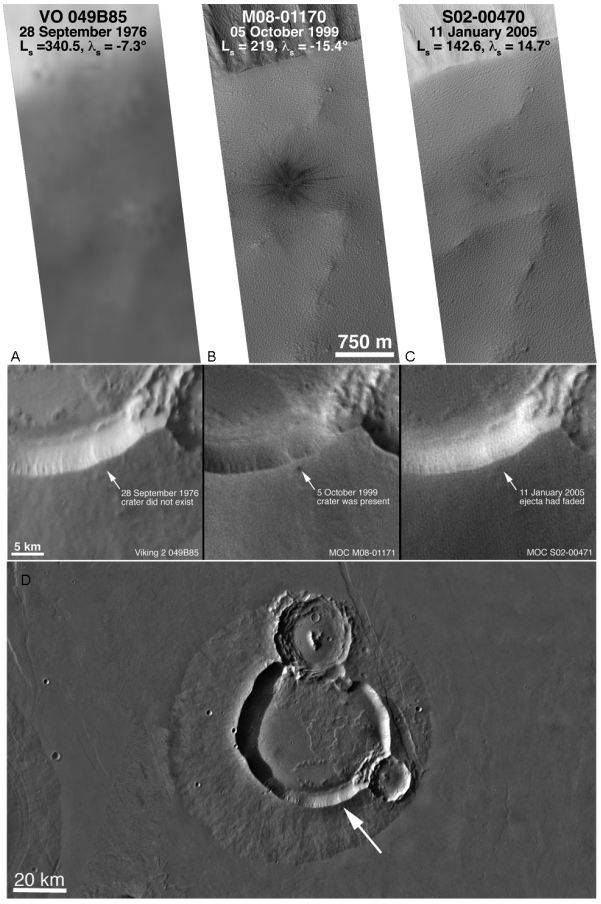

Figure 10.8.: Celebrating 8 years at Mars[1], the Malin Space Science Systems released images showing recent changes on Mars. One of these press releases (MOC2-1221) describes the possible formation of a small crater at the rim of Ulysses Patera (D) during the the 1980s, which is shown here. The upper row (A,B,C) shows the small crater with dark rayed ejecta in Viking imagery of 1976 recalculated to MOC resolution, where most likely no crater is present (A), and two MOC narrow–angle images of 1999 (B) and 2005 (C), indicating a fading in albedo of the ejecta during the last 6 years. The lower row shows the same Viking image in original resolution (A) and the MOC wide–angle context images (B, C).

10.4. Small–crater production on Mars observed by MGS

A recent press release, celebrating 8 years of the Mars Global Surveyor at Mars by the Malin Space Science Systems, describes the possible formation of a small crater at the rim of Ulysses Patera during the 1980s (Fig. 10.8) [1]. By comparing the location of the new crater in a Viking–2 orbiter image taken in 1976 with views taken by the Mars Global Surveyor (MGS) Mars Orbiter Camera (MOC) in 1999 and 2005. The new crater has a diameter of about 25 meters. The images indicate that the distinctly dark rayed ejecta pattern is fading somewhat away between 1999 and 2005.

Commonly, the cratering rate of Mars is determined by scaling from the lunar cratering rate, as discussed before. Long-term observations, e. g. from orbiting spacecraft, now allows the science community to actually locate new craters and possibly to derive cratering rates.

[1] http://www.msss.com/mars_images/moc/2005/09/20/

Based on the discovery of one crater that appears to have formed on Mars in the past 20 years, in addition to possibly several other similar craters, an estimate of the present cratering rate on Mars was given. They claim that the recent cratering rate on Mars is about 3 to 6 x 10^{-8} craters/km^2/year for craters between 25 and 100 m diameters. They argue it is about 5 times lower than previous estimates, although their sample is very small (the MOC narrow angle camera has only imaged just over 4 percent of Mars).

Applying the transferred lunar crater production function by Neukum (1983); Neukum and Ivanov (1994); Ivanov (2001) and the scaled lunar cratering rate (cratering chronology model by Hartmann and Neukum (2001)), about 1.2 x 10^{-7} craters of 25 m in diameter per km^2 and year (0.9 x 10^{-8}, 30 m) and about 1.5 x 10^{-9} craters of 100 m in diameter per km^2 and year would be produced. These results indicate the minima and maxima of the interval of the diameter range (25 to 100 m), and reflect the same frequency.

Considering the uncertainties of the statistically limited extrapolation by Malin, the rate transferred from the moon to Mars and the rate derived by Malin are in good agreement, and indicate that secondary cratering contamination does not invalidate the applied method of surface age determination. Moreover, this calculation given here shows that his argument that the cratering rates determined by Hartmann and Neukum (2001) from small craters are overestimated is wrong.

10.5. Conclusion

In the previous sections, basic assumptions led to the discussion of pros and cons of a secondary– or primary–generated steep distribution branch at the smaller size range. Most assumptions induce artificial crater size–frequency distribution mainly contradicting the measured crater size–frequency distribution. The confirmed measured Martian standard crater production function is given in the next chapter.

Estimates of the fraction of secondaries compared to the Martian standard crater production function, following commonly discussed assumptions, allows only for an entire –3–sloped secondary distribution at most. This is also in agreement with observations (e.g. König, 1977). In this case the percentage of secondary hypothetical global unrecognized craters is usually less than 5 % in any crater size–frequency distribution measurements. Any other hypothetical secondary crater distribution contradicts the observed distribution measurements, e.g. at about 3.7 Ga (compare Fig. 10.7, bottom, for the hypothetical percentage and an example measured at Ceraunius Tholus, Fig. XXXI, Appendix).

Conclusively, the measurements are "contaminated" by secondaries in percentage less than the statistical error assumed.